ARTICLE

Extraordinary Hydrogen Evolution and Oxidation Reaction Activity from Carbon Nanotubes and Graphitic Carbons

Rajib Kumar Das,[†] Yan Wang,[†,‡] Svetlana V. Vasilyeva,[†] Evan Donoghue,[†] Ilaria Pucher,[†] George Kamenov,[§] Hai-Ping Cheng,[†,‡] and Andrew G. Rinzler[†,*]

[†]Department of Physics, [‡]Quantum Theory Project, and [§]Department of Geological Sciences, University of Florida, Gainesville, Florida 32611-8440, United States

ABSTRACT The hydrogen evolution reaction, $2H^+ + 2e^- \rightarrow H_2$, and its converse, the hydrogen oxidation reaction, $H_2 \rightarrow 2H^+ + 2e^-$, are central to any realization of a hydrogen economy. Various forms of carbon have been used for decades as the precious metal catalyst support in these reactions. Here we report the unexpected result that single-wall carbon nanotubes and some graphitic carbons, activated by brief exposure to electrochemical potentials that induce hydrogen evolution in intercalating acids combined with extended soak times in such acids, acquire an activity for these reactions that exceeds that of known nonprecious metal catalysts.

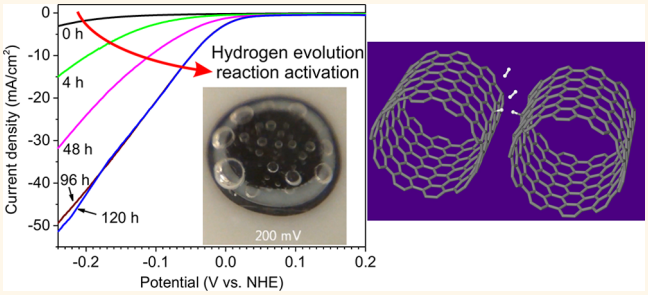

KEYWORDS: water splitting · hydrogen evolution · hydrogen oxidation · carbon nanotubes · graphitic carbons

The use of carbon as a catalyst support and its role in the hydrogen evolution reaction (HER) and in the hydrogen oxidation reaction (HOR) has been an intense subject of study since the early days of the U.S. space program in the 1960s. Much further research was stimulated by the oil shortages of the 1970s and 1990s and most recently by the increasingly recognized need for carbon-neutral energy sources/carriers. Despite carbon's seemingly synergistic enhancement of the activity of the metallic catalysts used in these electrochemical reactions, carbon itself has been reported to exhibit HER only at high overpotential and no HOR activity whatsoever.[1] Here we report that by simple exposure of single-wall carbon nanotubes (SWNTs) to acidic intercalants, in combination with low voltage electrochemical cycling, the material develops both HER and HOR activity that initiates at near zero overpotential, with an activity rivaling that of the best known nonprecious metal catalysts in these reactions. Of practical significance, the high activity for HER is shown to persist in pH-neutral aqueous electrolyte and in seawater. Our studies began with SWNTs; however, encouraged by those results, we have also found that similar activation can be induced in select forms of graphitic carbons.

Carbon nanotubes have been explored largely as scaffold supports for noble and non-noble metal catalytic particles and for enzymatic-inspired catalysts in HER and/or HOR.[2−9] Few studies have reported on water splitting for pure carbon nanotubes,[10,11] and none have reported the low overpotential activities demonstrated here. Our experiments rule out conventional metals as the source of the activity, and the results, in combination with density functional theory (DFT) modeling, lead to a proposed explanation.

RESULTS AND DISCUSSION

Figure 1a shows quasi-steady-state (5 mV/s) voltammograms of hydrogen evolution currents for a 1.5 μm thick SWNT film working electrode with 54 μg of SWNTs exposed to 1 M H_2SO_4. The black curve shows the initial behavior exhibiting a high overpotential for

* Address correspondence to rinzler@phys.ufl.edu.

Received for review June 3, 2014 and accepted July 11, 2014.

Published online July 11, 2014
10.1021/nn5030225

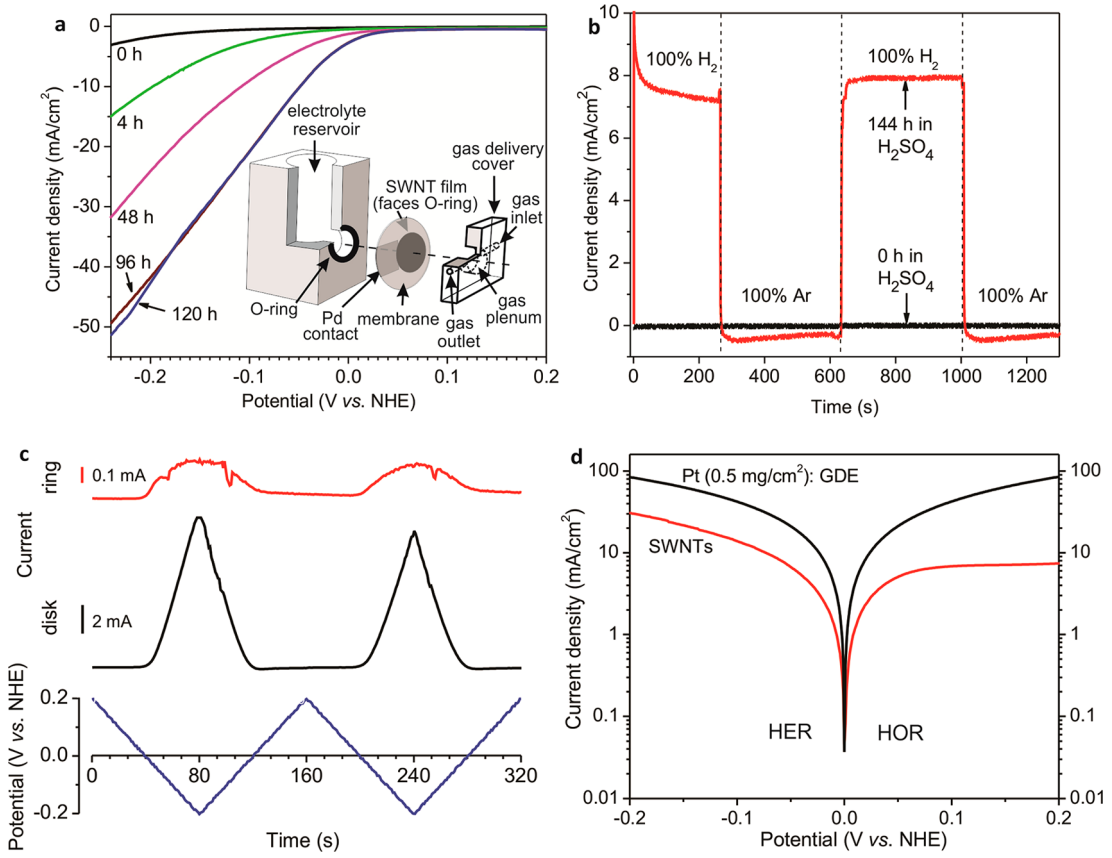

Figure 1. Hydrogen evolution and hydrogen oxidation reactions on the SWNT films (54 μg) before and after activation in 1 M H_2SO_4. (a) Quasi-steady-state voltammograms (5 mV/s) following the indicated time and electrochemical cycling in the acid, evidencing the increasing HER activity. The inset shows the custom-fabricated Teflon electrochemical cell used in these experiments. (b) Chronoamperometry at +0.3 V *vs* NHE immediately upon immersion in the acid (black) and after 144 h of activation (red) while exposing the film to 100% inert gas or 100% hydrogen at the times indicated, demonstrating the HOR activity induced by the activation. (c) RRDE data confirming that the cathodic currents are due to hydrogen evolution. The ring electrode was held at +0.6 V, while the activated SWNTs on the disk electrode were swept between ±0.2 V. Coincidence of the ring current beginning with the disk current indicates oxidation of the hydrogen evolved at the disk. (d) Tafel plots of the HER and HOR activity of the acid-activated SWNTs (red) compared to those of the commercial Pt-loaded electrode (black).

the onset of HER current. After recording this voltammogram, the working electrode potential was scanned cyclically from +0.2 to −0.7 V *vs* NHE at 50 mV/s. This was done for five consecutive scans followed by disconnection from the potentiostat for the time delay (as labeled in Figure 1a) until the next voltammogram was recorded (green curve). Such cycling followed by the long soak time constitutes the simple activation process, and both the brief exposure to potentials that cause H_2 evolution and the soak times were necessary to induce the observed changes in the activity. Repeating the process resulted ultimately in a saturation of the changes. Prior to each measurement, the electrolyte was purged with inert gas (argon) for 30 min. Between measurements, the reference electrode was stored in a separate container and rinsed with fresh DI water before each reuse. All cycling and measurements were done at room temperature. Steady-state measurements (with 10 min settling times) recorded at a few potentials validated the quasi-steady-state curves shown in Figure 1a. The inset to Figure 1a shows the experimental setup, which has the SWNT film deposited on a PTFE membrane, allowing the film to be wetted by the electrolyte on one side while being exposed to the desired gas through the gas plenum lying behind the membrane on the other (description in Methods and Supporting Information). In this set of HER measurements, the gas flowing through the plenum was argon (replaced by hydrogen for the HOR measurements discussed below). Shift of the onset potential and growth of the HER current with cycling and time of acid exposure is evident. At the end of this activation process, the onset of catalytic HER current has shifted to 0.0 V, corresponding to zero overpotential (applied potential minus thermodynamic potential of hydrogen evolution).

Figure 1b shows chronoamperometry in 1 M H_2SO_4 of a 1.5 μm thick SWNT film (54 μg of SWNTs exposed to the acid) at +0.3 V upon switching the gas fed to the plenum back and forth between hydrogen and inert gas (argon) before (black curve) and after 144 h of activation in the acid (red curve). Initially, the SWNTs show no HOR current with exposure to the hydrogen gas (black curve), while once activated, substantial HOR current appears (red curve).

Figure 1c shows rotating ring-disk electrode (RRDE) data, confirming that the cathodic currents are due to proton reduction (with H_2 evolution). In this case, the SWNTs (27 μg) were drop-cast from ethanol onto the 5 mm diameter glassy carbon (GC) disk electrode followed by activation in 1 M H_2SO_4 for 144 h prior to recording the data shown (control experiments on the GC disk electrode without nanotubes confirmed an overpotential for HER that remains high at ~ -500 mV *vs* NHE, under similar conditioning). Measurements were recorded in 1 M H_2SO_4 rotating at 1200 rpm. The disk potential was linearly swept at 5 mV/s between ± 0.2 V (lowest plot, blue). The center plot shows the disk reduction current (black), while the top curve shows the oxidation current (red) from the Pt ring held at $+0.6$ V, detecting the hydrogen. With the disk stationary, H_2 bubbles are already seen to evolve from the nanotube layer at -60 mV, becoming increasingly vigorous with increasing cathodic potential. The saturation seen in the hydrogen oxidation ring current is due to the increasing number of H_2 bubbles that physically separate the electrolyte from the ring on their excursion outward. The larger current dips correspond to the separation of particularly large bubbles.

Figure 1d shows the logarithmic current density as a function of overpotential for an activated SWNT film (54 μg) measured in 1 M H_2SO_4 (5 mV/s scan rate) in the electrochemical cell (inset Figure 1a) with H_2 flowing through the gas plenum (red curve). This is compared for the same measurement conditions against a Pt-loaded (0.5 mg/cm^2, 250 μg Pt exposed to the electrolyte) commercial gas diffusion electrode (GDE, ELAT HT140EW, The Fuel Cell Store) measured in place of the SWNT film with the platinized microporous layer facing the electrolyte (black curve). The activated SWNT electrode exhibits the transition from HER to HOR at 0.0 V potential *vs* NHE as does the Pt-loaded GDE corroborating the low overpotentials for initiating the reactions on the activated SWNTs. At -0.2 V, the HER current for the SWNTs is a remarkable 30 mA/cm^2 *versus* that for the Pt-loaded GDE of 86 mA/cm^2. At this low overpotential, the specific (mass basis) activity of the SWNTs is 278 A/g, actually exceeding that for the Pt-loaded electrode (which gives *under these conditions* 172 A/g). The hydrogen oxidation current at $+0.2$ V for the SWNT film is a substantial 7 mA/cm^2 (specific activity 65 A/g compared to the commercial Pt electrode's specific activity, *under these conditions*, of 168 A/g). On a rotating disk electrode, the 27 μg acid-activated SWNT layer rotating at 1400 rpm attains 58 mA/cm^2 of HER current at -0.2 V *vs* NHE, which corresponds to 422 A/g (Supporting Information).

To be clear, these results should not be misinterpreted as a claim that the SWNTs rival Pt in their activity. The commercial Pt-loaded GDE is optimized for use in a proton exchange membrane (PEM) fuel cell where, under the appropriate conditions of temperature, pressure, and humidity, they attain much higher current densities (by about an order of magnitude). The commercial Pt electrode performance here is typical for half-cell measurements in liquid acid electrolyte (*e.g.*, see Le Goff *et al.*[8]), where electrolyte impedance and diffusion limitations dominate. Nevertheless, both the 0.0 V activity onset *vs* NHE for the SWNTs (matching that of Pt) and the level of activity shown by the SWNTs is remarkable. Moreover, the same electrolyte impedance and diffusion limitations hold for the SWNT electrode. Indeed, while the commercial GDE has been highly engineered for a large surface area three-phase interface, the vacuum filtration method used in fabricating the SWNT films produces compact films, possessing only a small-channel, tortuous path porosity.[12] For the HOR reaction, this makes little of the SWNT film thickness accessible, which combined with the relatively low solubility of hydrogen in acid implies substantial room for improvement by porosity/hydrophobicity engineering. Similarly, on the hydrogen evolution side, H_2 bubbles trapped on and within the film pore volumes tend to cut off regions of the film, again suggesting significant margin for optimization. Due to the tortuous path nature of the SWNT films, we were unable to find clear linear regions in the Tafel plots to permit extraction of the Tafel slope and exchange current density. Attempts to activate very thin films on the glassy carbon RRD electrode for such purpose were frustrated by their delamination from the electrode. To make comparison with alternative nonprecious metal catalysts, at -0.2 V *vs* NHE (200 mV overpotential), the nickel bisdiphosphine catalyst recently reported by Le Goff *et al.* exhibited a hydrogen evolution (oxidation) current of $\sim$1.3 mA/cm^2 (0.9 mA/cm^2) for 60 μg/cm^2 of the catalyst yielding a specific activity of 22 A/g (15 A/g).[8] Amorphous molybdenum sulfide films were recently described as exhibiting HER current densities said to be "among the highest reported for non-noble catalysts".[13] At -200 mV, the current reported was 14 mA/cm^2, about a factor of 2 lower than the SWNT HER activity reported here. Long-term (10 h) measurements of the SWNT HOR and HER at $+300$ and -300 mV, respectively, show the high activity to be retained over the duration of the measurement (Supporting Information).

Water abundance on earth exists close to pH-neutral. Hence, for maximum utility in hydrogen production, it is desirable to have catalysts that function at low overpotential in the vicinity of pH 7 water. Figure 2a compares for HER the cyclic voltammetry (CV) of an acid-activated SWNT film in pH 7.2 phosphate buffer (0.6 M) to that for the Pt-loaded GDE. The solid tangent lines are drawn to aid in estimating the point at which the HER initiates for each electrode (dashed vertical lines). For the Pt-loaded electrode, this occurs at about -420 mV, while for the activated SWNTs, this occurs at -490 mV, giving an overpotential of 70 mV, which is still remarkably low. At 1.0 V overpotential, the SWNT film

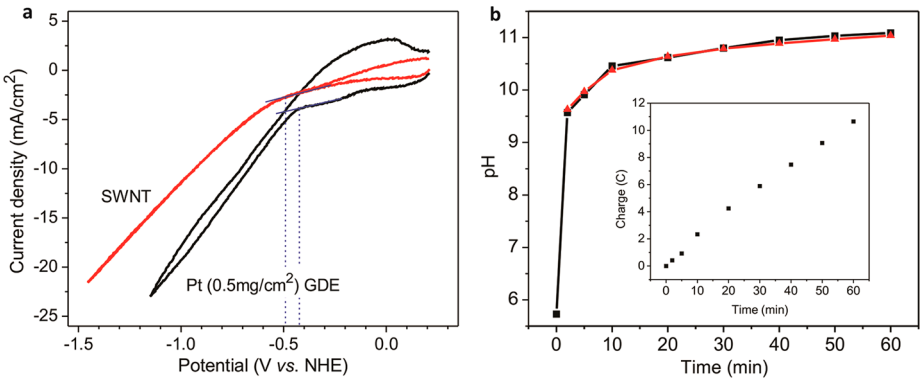

Figure 2. Hydrogen evolution at near-neutral pH. (a) CV of an acid-activated, 1.5 μm thick SWNT film in pH 7.2 phosphate buffer (0.6 M) (red) and the commercial Pt-loaded GDE under the same conditions (black) measured in the electrochemical cell. (b) Demonstration of the Faradaic efficiency for HER of the acid-activated SWNTs. Measured pH (black squares) of a stirred, unbuffered KCl solution as the HER proceeds at −1.4 V. The calculated pH of the solution based on the measured charge passed (inset) is shown as the red triangles.

TABLE 1. Reported Non-precious Metal HER Onset Overpotentials and Activities in near pH 7 Aqueous Electrolytes

catalyst	onset overpotential (V *vs* RHE)	current/geometric area at indicated overpotential	ref
nickel^{II}—cyclam[a]	~0.90	~0.01 mA/cm^2 at 1.0 V	14, 15
cobalt pentapyridine[a]	0.66	2.4 mA/cm^2 at 1.0 V	16
molybdenum—oxo complex[a]	0.52	9.1 mA/cm^2 at 1.0 V	17
cobalt nanoparticles from boron-capped tris(glyoximato) cobalt clathrochelate complex on GC	~0.1	20 mA/cm^2 at 0.7 V	18, 19
molybdenum sulfide/carbon composite on carbon cloth	0.11	1 mA/cm^2 at 0.80 V	20, 21
H_2—CoCat on FTO	0.05	3.3 mA/cm^2 at 0.45 V	22
activated SWNTs[b]	0.03	38 mA/cm^2 at 1.0 V	this work

[a] Molecular catalyst in solution. [b] With 3 M salt concentration from Supporting Information to minimize electrolyte impedance.

gives 22 mA/cm^2 HER current. The larger separation of the forward and reverse parts of the scan for the commercial electrode reflects the larger non-Faradaic capacitive charging due to the greater surface area of the commercial electrode compared to the relatively compact SWNT film. HER for the SWNTs in pH 6.4 buffer with a higher 3 M salt concentration shows the reaction to have an onset at a mere 30 mV overpotential and yields 38 mA/cm^2 of HER current at 1.0 V overpotential (Supporting Information). Table 1 compares values of the overpotential for the hydrogen evolution reaction onset and the current density at the given overpotential for the best reported nonprecious metal catalysts at neutral and near-neutral pH. A separate measurement of the pH change in initially near-neutral, *nonbuffered*, 1 M KCl solution confirms hydrogen evolution with 100% Faradaic efficiency. Figure 2b shows the measured changes in pH with time (black squares) and the calculated pH (red triangles) based on the corresponding measured charge (inset Figure 2b), assuming that each pair of electrons corresponds to the evolution of one hydrogen molecule (leaving behind a hydroxyl ion pair to raise the pH). Hydrogen evolution from filtered Atlantic seawater (without additives) is shown in the Supporting Information, demonstrating the activated SWNT electrode tolerance for impurities and robustness of its activity.

This degree of HER/HOR activity is remarkable only if it can be demonstrated that it does not originate from some conventional metal present in the SWNT material. Obvious candidates to rule out are the residual metals used to catalyze the nanotube growth. The graphitic targets in our dual pulsed laser vaporization grown SWNT material are loaded with 1 atom % each of nickel and cobalt. Following purification (nitric acid reflux/cross-flow filtration[23]), proton-induced X-ray emission (PIXE) shows these metals to be present at 0.05 atom % of the SWNT carbons. However, in accord with the Pourbaix diagrams,[24,25] these metals can only survive the SWNT purification (HNO_3 reflux), H_2SO_4 acid exposure during activation, and the acidic test conditions by virtue of being encased in bucky-onions, rendering the metal surfaces inaccessible as the catalytic sites. Nevertheless, to gain further confidence that these residual metals are not the source of the activity, the material was further purified by high-speed centrifugation. To measure the remaining, very low metal concentration, the material was incubated in Aqua Regia and the solution was injected into an inductively coupled plasma mass spectrometer (ICP-MS). This gave a residual Ni content of 0.0018 atom % of the SWNT carbons (the cobalt concentration was even lower). HER activation of films made from this material was

found to progress to the same degree, at the same rate as shown above, even though the material now contained a factor of 28 times less of these metals. For comparison, note that the commercial electrode exhibiting the HER/HOR shown in Figure 1d contains more highly catalytic Pt at the much higher concentration of ~2.6 atom % of its carbon support. That the trace Ni and/or Co remaining in our material should exhibit an activity approaching that of the highly optimized commercial Pt catalyst (albeit under diffusion-limited conditions) while being present at concentrations over 1000 times lower for each metal would require invoking some extraordinarily unlikely new catalytic form.

The counter electrode used in the preceding studies was platinum, which is generally the electrochemical material of choice. Under conditions of anodic cycling, however, Pt has been shown to exhibit minor (though non-negligible) dissolution.[26,27] The cathodic cycling of our SWNT working electrode during the activation constitutes anodic cycling for the Pt counter electrode, raising the possibility of anodically dissolved Pt redepositing onto the nanotubes and this Pt being the source of the observed activity. To minimize such concern, an experiment was performed in which the acid was discarded immediately following each day's set of electrochemical cycling, replacing it with fresh acid for the overnight soak and only replacing the counter electrode at the start of the next day's cycling, with no change in the resulting rate or degree of activation. The activation was also performed with the platinum counter electrode replaced by a gold electrode, which yielded the same results, but since other precious metals might be considered culpable in inducing the observed activity, we resolved to attempt the activation using a glassy carbon counter electrode. To additionally avoid the possibility of Ag contamination from the Ag/AgCl reference electrode, a double junction reference electrode was used, with the outer tube filled with fresh electrolyte and the inner Ag/AgCl reference inserted only immediately before each day's cycling, with the outer tube thoroughly rinsed and dried immediately after such cycling. The palladium contact pad, used above to make electrical connection to the SWNT working electrode (outside the electrolyte wetted area, inset Figure 1a), was replaced in this set of experiments by a thick (1.5 μm) SWNT film strip (itself connected to the potentiostat *via* a remote copper clip). To ensure that there was no incidental environmental contamination, all film fabrication and assembly steps were performed in a class 100 clean room; all labware used was first soaked in Aqua Regia for 30 min, and all chemicals and dilution/rinsewater used were of the highest available purity (Optima grade acids, from Fisher Scientific, TraceSELECT Ultra water from Fluka Analytical). Finally, ICP-MS was performed on a sample of the centrifuged SWNT material before and after the activation to look for Pt or Ag contamination (Methods).

In the first such attempted activation, the shifts in the onset potentials with cycling and soaking time were clearly evident, but the currents obtained were substantially lower. From the rapid appearance of a brownish film and flaking of the counter electrode, it soon became evident that the GC was being oxidized, limiting the currents. In the next attempt, the GC counter electrode was periodically polished (5 μm Al_2O_3 Micropolish, Buehler Inc.), followed by a thorough pure water rinse. Even so, we found that for the activation currents to approach the previous levels much more cycling (200–500 cycles) was required, with the GC counter electrode repolished every 50–100 cycles. Figure 3a shows the quasi-steady-state voltammograms (5 mV/s) following the indicated soak times in the acid. The major

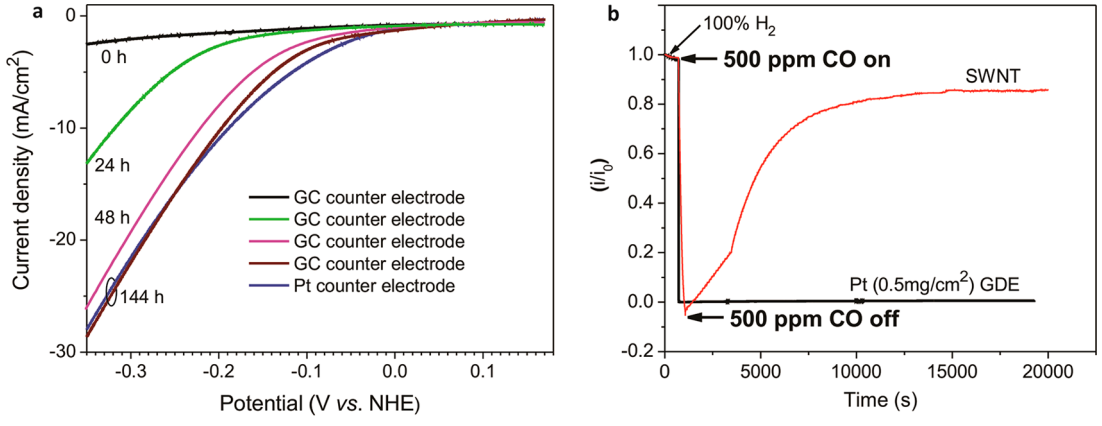

Figure 3. Evidence that conventional metals are not responsible for the observed catalytic activity. (a) Quasi-steady-state voltammograms (5 mV/s) following the indicated time in 1 M HNO_3 acid (see below) for a 600 nm thick SWNT film with cycling and measurements performed *versus* a GC counter electrode demonstrating metal-free HER activation. Also shown is the terminal activation using a Pt counter electrode for comparison. (b) Effect of CO exposure on the HOR for the Pt-loaded GDE (black line) and the acid-activated SWNTs (red line) at 50 mV overpotential in 1 M H_2SO_4. The comparatively rapid recovery of the SWNT HOR activity conclusively demonstrates that conventional metal catalysts are not the origin of the catalytic activity. At the break in the rise for the SWNT HOR current, the H_2 flow rate through the plenum, having dropped, was increased.

fraction of the activation is clearly demonstrated, despite the absence of a conventional metal counter electrode. ICP-MS of the Aqua Regia (4 mL) soaked SWNT material showed a quantity of Ag and Pt *before* the activation of 161 and 151 ppt, respectively. After the activation, the quantity of Ag and Pt detected were 94 and 129 ppt. All of these values are consistent with trace background levels and could not possibly account for the activated behavior observed.

Further conclusive evidence that conventional metal catalysts cannot be responsible for the observed activity is shown in Figure 3b, where the carbon monoxide sensitivity of the activated SWNTs undergoing HOR was tested and compared to that of Pt. The black curve shows the HOR current (normalized to the initial current) at 50 mV overpotential for the Pt-loaded, commercial GDE in 1 M H_2SO_4 upon the addition of 500 ppm of CO to the hydrogen flowing through the gas plenum (inset Figure 1a). As expected, the CO poisons the metallic catalyst so that even once the CO flow is terminated (returning to 100% H_2) the metallic catalyst remains inactive. The red curve shows the same experiment on an acid-activated SWNT film (Pt counter electrode used in that activation). The very high CO concentration also deactivates the SWNTs; however, upon switching back to pure H_2 the HOR activity immediately begins to recover. All conventional metallic particle catalysts would have been rendered inactive by the CO exposure (as was the Pt), demonstrating that conventional metals are not the source of the observed HOR activity or, by extension, the source of the HER activity. There exist natural hydrogenases that have exhibited a similar deactivation and recovery upon exposure to CO.[28] However, the idea that we could have accidentally created such an exotic catalyst, bound to the SWNTs in a manner that does not disrupt their electrical conductivity, and in the quantities necessary to exhibit the degree of activity shown, stretches credulity. Further corroborating evidence that conventional metals are not the source of this activity appears in the Supporting Information.

Sulfuric acid is a known spontaneous intercalant in SWNTs.[29] To test whether intercalation is relevant to the behavior, activation of samples was attempted in 1 M HNO_3 and 1 M HCl, the former a known charge transfer intercalant of sp^2-bonded carbons, while the latter is not. The acid exposure and low voltage cycling gave only a small increase of the HER currents in HCl, while activation in the HNO_3 was comparable to that in the H_2SO_4 (Supporting Information). Exposure to higher concentrations of HNO_3 (6 and 16 M) greatly accelerated the rate of the activation. SWNTs exposed to 16 M HNO_3 for 8 h and transferred to 1 M HNO_3 for subsequent cycling and measurements attained saturation HER currents (for any given voltage) within 8 h in the 1 M acid. Raman spectra of acid-activated and non-activated SWNT samples (Figure 4) show an upshift in the G band of 2.6 cm^{-1}, consistent with a moderate degree of intercalation upon activation.[24] The D/G band ratio in these samples shows a slight *decrease* of the ratio in the activated sample as is evident from the relative intensities of the D bands in Figure 4, where the spectra were normalized to the same G band peak intensities. This provides strong evidence that the activation does not induce additional defects or effect chemical functionalization of the nanotube sidewalls. It might be thought that the perceived increase in the activity corresponds merely to increased low level currents from the increased surface area made accessible due to the intercalation. This, however, cannot explain the dramatic shift in the overpotentials for the HER and HOR reactions (as discussed further in the Supporting Information). Given all of this evidence, we are led to the working hypothesis that the SWNTs themselves are responsible for this remarkable HER/HOR activity.

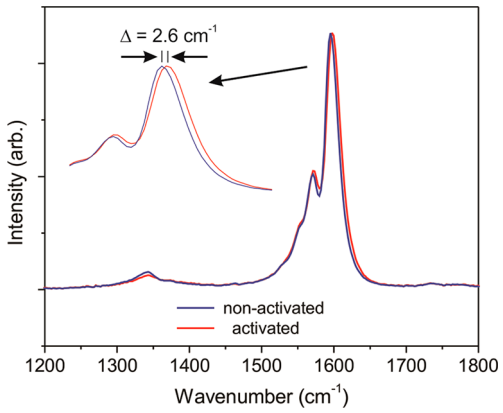

Figure 4. Raman spectra of the D and G band regions for a nanotube film used in the cell of Figure 1. Spectra normalized to the same G band peak intensity. Inset is a zoom on the G band peak showing the upshift of the peak on activation due to charge transfer associated with the acid intercalation.

DFT modeling can provide valuable insight into molecular scale processes not directly accessible by experiment. Details of the modeling are provided in the Supporting Information; here we summarize the findings. Simulation of the steps relevant to HER shows that (1) a hydronium ion surrounded by a water cluster[30] in the vicinity of a (10,10) SWNT sidewall has a large barrier for transfer of the proton to a chemisorbed, discharged state on the carbon lattice (Volmer association step). Such a barrier is consistent with the published Tafel slope for HER on highly ordered pyrolytic graphite (HOPG) in H_2SO_4, found to be 120 mV/decade of current,[31] which indicates chemisorption of the proton (and its discharge) to be the rate-limiting step. Electrons added in the simulations to the SWNT (consistent with increasing cathodic potential) are found to reduce this barrier. (2) For two hydrogen atoms that are already chemisorbed at first, second, or third nearest neighbor sites on the hexagonal lattice, there is a substantial barrier for

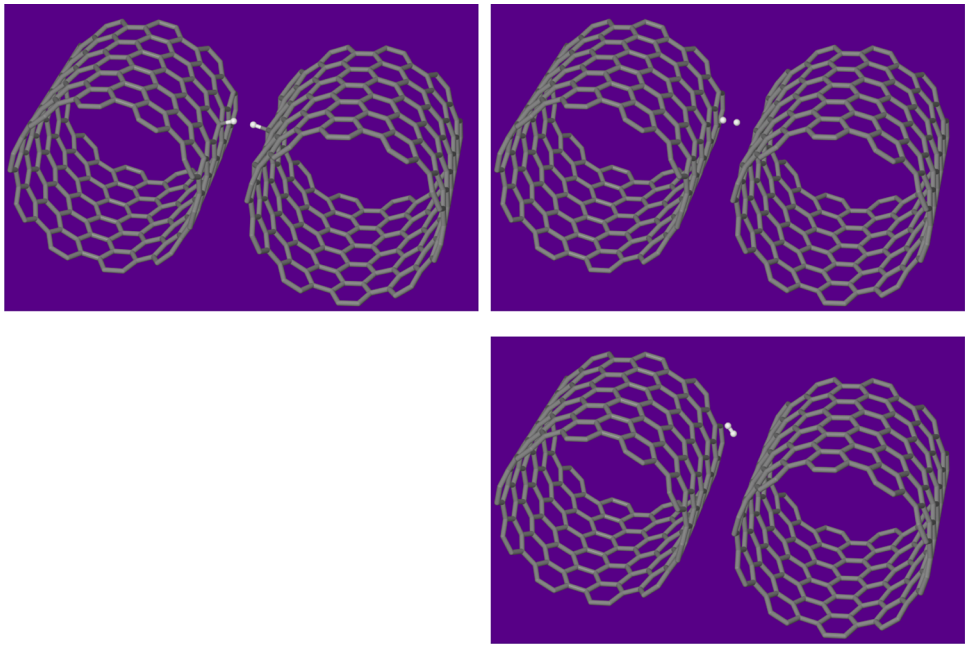

Figure 5. Proposed adjacent Tafel mechanism. DFT calculations show that two hydrogen atoms chemisorbed in proximity on two adjacent nanotubes have to overcome only a small activation barrier to form a hydrogen molecule (details Supporting Information).

association of the two hydrogen atoms (remaining large even with electrons added to the SWNT upon charging). This would seem to preclude the so-called Tafel mechanism $H_{chm} + H_{chm} \rightarrow H_2$; however, the existence of layered systems (the nanotubes exist predominantly in bundles) provides another route to such a process: the two hydrogens can be chemisorbed in close proximity on adjacent nanotubes. That circumstance gives a relatively small barrier to this mechanism, which we designate "adjacent Tafel" (Figure 5). (3) Finally, the Heyrovsky mechanism, in which a hydronium ion yields a proton directly to a hydrogen atom chemisorbed to the sp^2 carbon lattice ($H_{chm} + H^+ + e^- \rightarrow H_2$), has a substantial barrier, which however also decreases as electrons are added to the lattice with increasing cathodic potential.

With this information, the following picture emerges. Hydrogen evolution from non-activated SWNTs is rate-limited not only by a barrier for chemisorption on the sp^2-bonded basal plane (Volmer step) but also by barriers for the Tafel and Heyrovsky mechanisms for desorption. For carbon nanotube bundles, the "adjacent Tafel" mechanism is available in the vicinity of the contact line between adjacent nanotubes on the outer surface of nanotube bundles, but the fraction of such sites that are populated in light of the slow chemisorption is not great. With increasing cathodic potential, electrons are added to the bundles but the rate of their addition is such that substantial overpotential is required before the onset of H_2 evolution, explaining the initial non-activated behavior. Low voltage cycling in intercalating acids accelerates the rate of spontaneous intercalation. Such moderate intercalation opens up the galleys between adjacent nanotubes in the bundles. Ions can now infiltrate these spaces between the nanotubes. In addition to the substantially larger surface area now made available for reaction, *and this is key*, the charge compensation provided by these intercalated but not chemisorbed ions increases the rate at which charge can be added to the nanotubes as the cathodic potential increases. This additional charge induced on the nanotubes, *compensated by the surrounding ions*, is analogous to the double-layer charging that gives electrolytic capacitors their high capacitance. As shown by the DFT modeling, this additional charging reduces the barrier to chemisorption, allowing the subsequent adjacent Tafel (note the close quarters between nanotubes in bundles) and the Heyrovsky reactions to proceed at low overpotential. This is true even for the outermost nanotubes of the bundles which can now have ions surrounding them on their previously inaccessible bundled inner sides. Further modeling and experiments are necessary for confirmation, but this picture is consistent with the results obtained to date.

Graphitic Carbons. These results for the SWNTs and our proposed mechanism suggested the possibility of inducing a similar activation in certain forms of graphitic carbons. The premise here being that near graphitic step edges, and at the edge "plane" of graphitic crystals, acid intercalation would locally splay apart the graphene sheets, giving electrolyte ions local access to *both sides* of the sheets. DFT modeling of graphene sheets in the relevant reactions (Supporting Information) showed that the barriers to proton chemisorption (Volmer process) and evolution by the adjacent Tafel and Heyrovsky processes are (like for

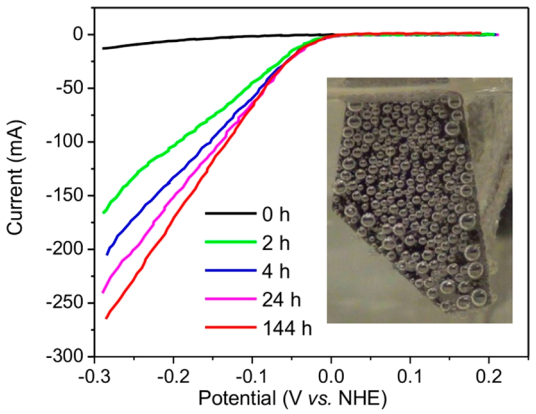

Figure 6. Activation of HOPG. Voltammograms recorded over the course of activating a piece of HOPG. Inset: hydrogen bubbles developing at −200 mV overpotential on the fully activated HOPG electrode.

the SWNTs) dramatically lowered by charge added to the graphene sheets. Thus, as for the SWNTs, the introduction of ions to previously inaccessible regions of the graphene layers would yield enhancement of the local double-layer capacitance, allowing for enhanced local charge addition and corresponding reduction of the barriers to these reactions.

Figure 6 shows voltammograms recorded, at the times indicated, during the activation of a piece of HOPG in 1 M HNO_3. The inset shows a photograph of H_2 bubbles developing on the *c*-plane of this HOPG (5.8 cm^2 face area × ~0.23 mm thick) at −200 mV overpotential following the activation. The idealized *c*-face is a single graphene sheet that would preclude our mechanism, but in reality, it of course contains many step edges. We have also found that some, though not all, carbon rod electrodes, comprised typically of microcrystalline graphitic particles held together by a pyrolyzed binder, can be activated. In particular, 3.18 mm diameter graphite electrode rods from Bay Carbon could be activated (Supporting Information and movie: Rods-HER-at-90-200-400 mV), while graphite electrodes from Electron Microscopy Sciences and Poco Graphite EDM grade 3 behaved like the glassy carbon electrodes and did not activate. For the Bay Carbon electrode rods that could be activated, a 400 °C bake in argon was effective at deactivating the rod, after which the activation could again be induced by our procedures. Other materials that we have found could be activated by this process were highly graphitized (heat treated to 3000 °C) carbon nanofibers obtained from Pyrograph and a Rayon derived carbon felt (heat treated to 1400 °C) from Alpha Aesar. The Pyrograph CNFs have a structure sometimes referred to as stacked cup carbon nanotubes; less information is provided by Alpha Aesar about their carbon felt material structure. Ongoing analysis of the microstructural differences between these materials and XPS studies may provide further insights into the mechanism. Our ongoing investigation of the activation with these other carbons has also revealed that it occurs not only with electrochemical cycling but also with the use of constant or pulsed potentials. What is important is that applied potential be made sufficiently negative for some degree of hydrogen evolution to initiate.

CONCLUSIONS

Our proposed mechanism for the activation may not be the complete story. Acid intercalation in SWNTs is a rapid process that does not take days, but such time scales are necessary for reaching the saturation level of activation, and electrochemical potentials that initiate H_2 evolution are also critical. While we have performed experiments designed to exclude precious metals from having access to the working electrodes, reduction below some persistent background level, measured in parts per trillion, is not possible. If that trace metal is somehow responsible for the activity observed, the discovery remains important, even if only from the perspective of a remarkable efficiency in precious metal utilization. Irrespective of the complete explanation at this early stage, these results have important practical significance. The principle carbon-neutral energy sources (solar, wind, and wave energy) have natural interruptions that require an efficient means for storage and recovery of their energy.[32,33] The generation of hydrogen from water by electrolysis and reconversion to energy and water in a fuel cell has an ideal thermodynamic efficiency of 83% for recovery of the electrical energy, higher if the fuel cell waste heat is also put to work.[34] This makes for an attractive energy storage and recovery solution. Finely divided platinum and its alloys catalyze the necessary reactions with minimum overpotential and thus permit the closest approach to the thermodynamic efficiency. The scarcity of Pt, reflected in its high cost, however, makes broad implementation prohibitive. Alternative, inexpensive catalysts that possess high efficiency in the necessary reactions have accordingly been highly sought after.[15,35] The activated carbons reported here may provide that long sought solution.

METHODS

Materials. Nanotubes used in these studies were dual pulsed laser vaporization synthesized and purified by nitric acid reflux followed by cross-flow filtration. Films of the purified nanotubes were formed from Triton X-100 surfactant suspensions filtered onto 200 nm pore PTFE membranes (Sartorious). Water washing removed the surfactant, and drying consolidated the film on the membrane surface.

The highly ordered pyrolytic graphite used was a piece of high-quality (low mosaic spread) HOPG random cutting from

the fabrication of X-ray monochromator crystals (Union Carbide, Ohio) provided by Prof. David Tanner, University of Florida.

Microcrystalline graphitic rods tested were from Bay Carbon (grade ST-21), impurities reported to be 1 ppm of Si and ≪1 ppm of Al, Ca, B, Fe, and Mg; Electron Microscopy Sciences (part number 70200); and Poco Graphite, EDM grade 3.

Carbon nanofibers were from Pyrograph (Pyrograph-III PR-24 XT-HHT). Rayon derived carbon felt was from Alpha Aesar (#43199).

The 0.5 mg Pt/cm^2 (30 wt % Pt) commercial Pt-loaded gas diffusion electrode was obtained from the Fuel Cell Store.

Reagents were from Fisher Scientific, ACS reagent grade, and used as received. In the metals-free activation experiments, the acids were Optima grade (Fisher Scientific) and the water was TraceSELECT Ultra water (Fluka Analytical).

Electrochemical Measurements. Potentials are reported relative to the normal hydrogen electrode (NHE) by the addition of 210 mV to the Ag/AgCl (3 M KCl) reference electrode used in the Teflon cell (description below) or by the addition of 197 mV to the Ag/AgCl (saturated KCl) reference electrode used in the RRDE cell. RRDE measurements were performed using a Pine Instruments AFCBP1 bipotentiostat, AFMSRCE rotator with an E6 series RRDE with a Pt ring, and glassy carbon disk. Linear sweep and cyclic voltammograms measured in the specially constructed electrochemical cell were recorded using a Gamry Reference 600 potentiostat. Faradaic efficiency measurements were performed in the RRDE setup, keeping the solution well stirred by rotating at 1600 rpm. The pH was measured using a Denver Instrument model 220 meter.

Specially Constructed Teflon Electrochemical Cell. Figure S1 (Supporting Information) shows a photograph of the Teflon electrochemical cell (schematic shown in the Figure 1a inset). Nanotube films used with this were formed by vacuum filtering SWNTs from aqueous surfactant suspension to the surface of a PTFE membrane, washing with DI water, and drying. The use of an oversized membrane (47 mm diameter) in the filter funnel allowed for the 15 mm diameter SWNT film to be offset to one side of the membrane. Except for the completely metal-free activation experiment (described in the article), electrical contact was provided by a Pd metal contact pad sputtered across the longer bare membrane surface to one edge of the SWNT film (with ~2 mm of overlap). The nanotube film side of the membrane was pressed to a circular opening in the sidewall of the electrochemical cell (inset Figure 1a). An O-ring surrounding the opening defined the working area (0.50 cm^2) of the SWNT film exposed to the electrolyte, with the Pd metal kept well outside the electrolyte wetted region. The nanotube film and its supporting PTFE membrane were pressed to the cell body O-ring by the gas delivery cover. The cover incorporated a gas plenum behind the membrane, directly in line with the opening in the cell body. Hydrophobicity of the PTFE membrane prevented the aqueous electrolyte in the reservoir (contacting the SWNTs) from seeping through the membrane to the plenum, while gases fed to the plenum diffused through the membrane to the SWNTs. Not shown in the Figure 1a inset are a Pt flag counter electrode, a Ag/AgCl reference electrode, and inert gas (Ar) purge lines that entered the electrolyte compartment through a lid that otherwise sealed the cell (cover shown in Figure S1).

Rotating Ring Disk Electrode Setup. For the rotating ring disk electrode measurements, nanotubes (27 μg) were drop-cast from ultrasonicated ethanol suspension onto the glassy carbon disk (5 mm o.d.). The GC disk was mounted into an RRDE assembly with a Pt ring (6.5 mm i.d., 7.5 mm o.d., Pine Instruments). Figure S2 (Supporting Information) shows the experimental setup.

Raman Spectroscopy. Spectra were recorded in a Renishaw Ramascope 1000, using 532 nm excitation and 1 mW power. Four spectra were recorded at distinct positions within the region that had been exposed to the acid during cycling, that is, within the region bounded by the O-ring (activated), and four spectra were recorded at distinct positions well outside the region defined by the O-ring (non-activated). Besides a consistent peak upshift and a slightly reduced D/G band ratio in the activated region spectra, the spectra recorded there were also consistently lower in intensity by a factor of ~1.6. This provides further evidence for the intercalation: the resonant Raman intensity depends on the electronic transition rate which is reduced by a partial ground-state depletion upon charge transfer intercalation/doping. Given the consistent differences between the spectra in the two regions the four spectra common to each region were summed and normalized to the same G band peak intensity, with the results shown in Figure 4.

ICP-MS. All reagents used for the ICP-MS elemental analyses were Optima grade, and the sample preparation was done under a clean lab environment in the Department of Geological Sciences at the University of Florida. SWNT material was leached in precleaned Savillex PFA vials (http://www.savillex.com) with Aqua Regia (3 mL of HCl and 1 mL of HNO_3) overnight on a hot plate at 120 °C. Under these conditions, it is expected that the elements of interest were transferred quantitatively into solution. After digestion, part of the Aqua Regia solution was further diluted with 5% HNO_3 and loaded in the ICP-MS for analysis. Elemental analyses were performed on a ThermoFinnigan Element2 HR-ICP-MS in medium resolution mode. Quantification of results was done by external calibration using a combination of commercially available standards (http://www.qcdanalysts.com) gravimetrically diluted to appropriate concentrations.

Conflict of Interest: The authors declare the following competing financial interest(s): The University of Florida has filed for patent on the use of the relevant carbons in hydrogen evolution and oxidation.

Acknowledgment. We thank Dr. Bhabendra Pradhan for useful discussions. R.K.D., S.V.V., E.D., I.P., and A.G.R. acknowledge support from Nanoholdings LLC. Y.W. and H.-P.C. acknowledge support from the NSF (DMR 0804407) and acknowledge the DOE/NERSC and the UF-HPC center for providing computational resources.

Supporting Information Available: Additional discussion; Figures S1−S19; movie: rods-HER-at-90-200-400 mV (description in SI pdf). This material is available free of charge *via* the Internet at http://pubs.acs.org.

REFERENCES AND NOTES

1. Kinoshita, K. *Carbon: Electrochemical and Physicochemical Properties*; Wiley: New York, 1988.
2. Carmo, M.; Paganin, V. A.; Rosolen, J. M.; Gonzalez, E. R. Alternative Supports for the Preparation of Catalysts for Low-Temperature Fuel Cells; The Use of Carbon Nanotubes. *J. Power Sources* **2005**, *142*, 169–176.
3. Lianga, Y.; Zhang, H.; Yi, B.; Zhang, Z.; Tan, Z. Preparation and Characterization of Multi-walled Carbon Nanotube Supported PtRu Catalysts for Proton Exchange Membrane Fuel Cells. *Carbon* **2005**, *43*, 3144–3152.
4. Girishkumar, G.; Rettker, M.; Underhile, R.; Binz, D.; Vinodgopal, K.; McGinn, P.; Kamat, P. V. Single-Wall Carbon Nanotube-Based Proton Exchange Membrane Assembly for Hydrogen Fuel Cells. *Langmuir* **2005**, *21*, 8487–8494.
5. Tang, J. M.; Jensen, K.; Waje, M.; Li, W.; Larsen, P.; Pauley, K.; Chen, Z.; Ramesh, P.; Itkis, M. E.; Yan, Y.; *et al.* High Performance Hydrogen Fuel Cells with Ultralow Pt Loading Carbon Nanotube Thin Film Catalysts. *J. Phys. Chem. C* **2007**, *111*, 17901–17904.
6. Grigoriev, S. A.; Millet, P.; Fateev, V. N. Evaluation of Carbon-Supported Pt and Pd Nanoparticles for the Hydrogen Evolution Reaction in PEM Water Electrolysers. *J. Power Sources* **2008**, *177*, 281–285.
7. Paunovi, P.; Dimitrov, A. T.; Popovski, O.; Slavcheva, E.; Grozdanov, A.; Lefterova, E.; Petrusevski, G.; Jordanov, S. H. Effect of Activation/Purification of Multiwalled Carbon Nanotubes (MWCNTs) on the Activity of Non-Platinum Based Hypo-Hyper d-Electrocatalysts for Hydrogen Evolution. *Mater. Res. Bull.* **2009**, *44*, 1816–1821.
8. Le Goff, A.; Artero, V.; Jousselme, B.; Guillet, N.; Métayé, R.; Fihri, A.; Palacin, S.; Fontecave, M. From Hydrogenases to Noble Metal-Free Catalytic Nanomaterials for H_2 Production and Uptake. *Science* **2009**, *326*, 1384–1387.

9. Svedružic, D.; Blackburn, J. L.; Tenent, R. C.; Rocha, J. D.; Vinzant, T. B.; Heben, M. J.; King, P. W. High-Performance Hydrogen Production and Oxidation Electrodes with Hydrogenase Supported on Metallic Single-Wall Carbon Nanotube Networks. *J. Am. Chem. Soc.* **2011**, *133*, 4299–4306.
10. Misra, A.; Giri, J.; Daraio, C. Hydrogen Evolution on Hydrophobic Aligned Carbon Nanotube Arrays. *ACS Nano* **2009**, *3*, 3903–3908.
11. Prosini, P. P.; Pozio, A.; Botti, S.; Ciardi, R. Electrochemical Studies of Hydrogen Evolution, Storage and Oxidation on Carbon Nanotube Electrodes. *J. Power Sources* **2003**, *118*, 265–269.
12. Das, R. K.; Liu, B.; Reynolds, J. R.; Rinzler, A. G. Engineered Macroporosity in Single-Wall Carbon Nanotube Films. *Nano Lett.* **2009**, *9*, 677–683.
13. Merki, D.; Fierro, S.; Vrubel, H.; Hu, X. Amorphous Molybdenum Sulfide Films as Catalysts for Electrochemical Hydrogen Production in Water. *Chem. Sci.* **2011**, *2*, 1262–1267.
14. Collin, J.-P.; Jouaiti, A.; Sauvage, J.-P. Electrocatalytic Properties of Ni(cyclam)$^{2+}$ and Ni_2(biscyclam)$^{4+}$ with Respect to Carbon Dioxide and Water Reduction. *Inorg. Chem.* **1988**, *27*, 1986–1990.
15. Cook, T. R.; Dogutan, D. K.; Reece, S. Y.; Surendranath, Y.; Teets, T. S.; Nocera, D. G. Solar Energy Supply and Storage for the Legacy and Nonlegacy Worlds. *Chem. Rev.* **2010**, *110*, 6474–6502.
16. Sun, Y.; Bigi, J. P.; Piro, N. A.; Tang, M. L.; Long, J. R.; Chang, C. J. Molecular Cobalt Pentapyridine Catalysts for Generating Hydrogen from Water. *J. Am. Chem. Soc.* **2011**, *133*, 9212–9215.
17. Karunadasa, H. I.; Chang, C. J.; Long, J. R. A Molecular Molybdenum−Oxo Catalyst for Generating Hydrogen from Water. *Nature* **2010**, *464*, 1329–1333.
18. Anxolabéhère-Mallart, E.; Costentin, C.; Fournier, M.; Nowak, S.; Robert, M.; Savéant, J.-M. Boron-Capped Tris(glyoximato) Cobalt Clathrochelate as a Precursor for the Electrodeposition of Nanoparticles Catalyzing H_2 Evolution in Water. *J. Am. Chem. Soc.* **2012**, *134*, 6104–6107.
19. Artero, V.; Chavarot-Kerlidou, M.; Fontecave, M. Splitting Water with Cobalt. *Angew. Chem., Int. Ed.* **2011**, *50*, 7238–7266.
20. Thoi, V. S.; Sun, Y.; Long, J. R.; Chang, C. J. Complexes of Earth-Abundant Metals for Catalytic Electrochemical Hydrogen Generation under Aqueous Conditions. *Chem. Soc. Rev.* **2013**, *42*, 2388–2400.
21. Tokash, J. C.; Logan, B. E. Electrochemical Evaluation of Molybdenum Disulfide as a Catalyst for Hydrogen Evolution in Microbial Electrolysis Cells. *Int. J. Hydrogen Energy* **2011**, *36*, 9439–9445.
22. Cobo, S.; Heidkamp, J.; Jacques, P.-A.; Fize, J.; Fourmond, V.; Guetaz, L.; Jousselme, B.; Ivanova, V.; Dau, H.; Palacin, S.; *et al.* Janus Cobalt-Based Catalytic Material for Electrosplitting of Water. *Nat. Mater.* **2011**, *11*, 802–807.
23. Rinzler, A. G.; Liu, J.; Dai, H.; Nikolaev, P.; Huffman, C. B.; Rodriguez-Macias, F. J.; Boul, P. J.; Lu, A. H.; Heymann, D.; Colbert, D. T.; *et al.* Large-Scale Purification of Single-Wall Carbon Nanotubes: Process, Product, and Characterization. *Appl. Phys. A: Mater. Sci. Process.* **1998**, *67*, 29–37.
24. Beverskog, B.; Puigdomenech, I. Revised Pourbaix Diagrams for Nickel at 25−300 °C. *Corros. Sci.* **1997**, *39*, 969–980.
25. Powell, D.; Cortez, J.; Mellon, E. K. Laboratory Exercise Introducing Students to the Pourbaix Diagram for Cobalt. *J. Chem. Educ.* **1987**, *64*, 165–167.
26. Llopis, J.; Sancho, A. Electrochemical Corrosion of Platinum in Hydrochloric Acid. *J. Electrochem. Soc.* **1961**, *108*, 720–726.
27. Rand, D. A. J.; Woods, R. A. Study of the Dissolution of Platinum, Palladium, Rhodium and Gold Electrodes in 1 M Sulphuric Acid by Cyclic Voltammetry. *J. Electroanal. Chem.* **1972**, *35*, 209–218.
28. Jones, A. K.; Sillery, E.; Albracht, S. P. J.; Armstrong, F. A. Direct Comparison of the Electrocatalytic Oxidation of Hydrogen by an Enzyme and a Platinum Catalyst. *Chem. Commun.* **2002**, *8*, 866–867.
29. Sumanasekera, G. U.; Allen, J. L.; Fang, S. L.; Loper, A. L.; Rao, A. M.; Eklund, P. C. Electrochemical Oxidation of Single Wall Carbon Nanotube Bundles in Sulfuric Acid. *J. Phys. Chem. B* **1999**, *103*, 4292–4297.
30. Hodges, M. P.; Wales, D. J. Global Minima of Protonated Water Clusters. *Chem. Phys. Lett.* **2000**, *324*, 279–288.
31. Despic, A. R.; Drzic, D. M.; Savic-Maglic, G. A.; Atanasoski, R. T. Hydrogen Evolution of Pytolytic Graphite. *Croat. Chem. Acta* **1972**, *44*, 79–87.
32. Lewis, N. S. Toward Cost-Effective Solar Energy Use. *Science* **2007**, *315*, 798–801.
33. Lewis, N. S.; Nocera, D. G. Powering the Planet: Chemical Challenges in Solar Energy Utilization. *Proc. Natl. Acad. Sci. U.S.A.* **2006**, *103*, 15729–15735.
34. Sherif, S. A.; Barbir, F.; Veziroglu, T. N. Wind Energy and the Hydrogen Economy—Review of the Technology. *Sol. Energy* **2005**, *78*, 647–660.
35. Cracknell, J. A.; Vincent, K. A.; Armstrong, F. A. Enzyme as Working or Inspirational Electrocatalysts for Fuel Cells and Electrolysis. *Chem. Rev.* **2008**, *108*, 2439.